MNRAS **000**, 1–15 (2019) Preprint 22 November 2019 Compiled using MNRAS LATEX style file v3.0

Formation of close binaries by disc fragmentation and migration, and its statistical modeling

Andrei Tokovinin,[1⋆] and Maxwell Moe[2]
[1] *Cerro Tololo Inter-American Observatory, Casilla 603, La Serena, Chile*
[2] *Steward Observatory, University of Arizona, 933 N. Cherry Ave., Tucson, AZ 85721, USA*

Accepted XXX. Received YYY; in original form ZZZ

ABSTRACT

Joint statistics of periods and mass ratios of close binaries and its dependence on primary mass can be explained by assuming that seed binary companions are formed by disc fragmentation at random intervals during assemblage of stellar mass and migrate inwards as they accrete from the circumbinary disk. A toy model based on simple prescriptions for the companion growth and migration reproduces such aspects of close solar-mass binaries as the distribution of binary periods P, the brown dwarf desert at short P, the nearly uniform distribution of mass ratios, and a population of equal-mass binaries (twins) that decreases linearly in frequency with $\log P$. For massive stars, the model predicts a large fraction of early mergers, a distribution of $\log P$ with a negative slope, and a mass-ratio distribution that is also uniform but with a substantially reduced twin fraction. By treating disc fragmentation as a stochastic process, we also reproduce the observed properties of compact triples. Success of our toy model suggests that most close binaries and compact triples indeed formed by disc fragmentation followed by accretion-driven inward migration.

Key words: binaries: general – binaries: close – stars: formation

1 INTRODUCTION

It is generally accepted that most binary stars form by fragmentation of proto-stellar cores or circumstellar discs (Bate et al. 1995; Kroupa 1995; Bate et al. 2002; Tohline 2002; Kratter & Matzner 2006; Clarke 2009; Offner et al. 2010; Kratter & Lodato 2016; Moe & Di Stefano 2017; Moe et al. 2019) In both cases, the initial separations cannot be less than ∼10 au because of the opacity limit to fragmentation (Boss 1986; Bate 1998). The first hydrostatic cores form with radii of a few au, and fragmentation during the secondary collapse phase is unlikely (Bate 1998, 2011). At such close separations, the accreting gas is generally too hot to become self-gravitating and fragment. Even if the opacities were smaller, e.g., at lower metallicities, any small density perturbations in the gas would quickly redistribute because the Keplerian orbital periods are shorter than the cooling timescales (Moe et al. 2019). The observed population of close binaries with $a \lesssim 10$ au must have initially fragmented at wider separations and subsequently migrated inward (Bate et al. 2002).

In very dense environments like globular clusters, close binaries may form via tidal capture, disk capture, and/or N-body dynamical interactions (Press & Teukolsky 1977; Murray et al. 1991; Hurley et al. 2007; Sollima 2008). Close field binaries, which formed in low density environments, require an alternative explanation for inward migration, such as hydrodynamical forces and torques in a circumbinary disk, orbital decay from protostellar accretion, and gravitational interactions in triple stars (Artymowicz 1983; Artymowicz et al. 1991; Bate et al. 1995; Bate & Bonnell 1997; Eggleton & Kisseleva-Eggleton 2006; Reipurth & Clarke 2001). The majority of solar-type binaries with semimajor axis $a = 0.1$ - 10 au do not have additional companions (Tokovinin et al. 2006; Tokovinin 2014), and so most close binaries migrated without the assistance of triple star interactions. Meanwhile, a significant majority of very close solar-type binaries with $P \lesssim 10$ days ($a \lesssim 0.1$ au) have tertiary companions (Tokovinin et al. 2006). Eggleton & Kisseleva-Eggleton (2006) suggested Kozai-Lidov interactions in misaligned triple stars, coupled to tidal friction, produce such very close pairs. Assuming all triple stars have random orientations, Fabrycky & Tremaine (2007) and Naoz & Fabrycky (2014) simulated Kozai-Lidov interactions for 10 Gyr and matched the observed properties of very close binaries.

However, Moe & Kratter (2018) showed that this mechanism can generate only a small fraction of very close binaries due to two main effects. First, the majority of compact triples, especially those with outer tertiaries $a_{\rm out} < 10$ au (below the opacity limit), actually have quasi-planar archi-

⋆ E-mail: atokovinin@ctio.noao.edu

tectures (Borkovits et al. 2016; Tokovinin 2017). Not only does this severely limit the fraction of triples that undergo Kozai-Lidov oscillations, but points to the dominant role of disk fragmentation and migration in the formation of close binaries and compact triples (see also Tobin et al. 2016). Second, Moe & Kratter (2018) noted that the very close binary fractions of solar-mass pre-main-sequence (pre-MS) and field binaries are nearly identical (Mathieu 1994; Melo 2003). In particular, Kounkel et al. (2019) recently demonstrated that class II/III T Tauri stars exhibit the same binary fraction and period distribution below $P < 10^4$ days ($a < 10$ au) as their field counterparts, with at most a ≈30% deficit at the shortest of periods $P < 5$ days. Close binaries with $a < 10$ au and the majority of very close binaries with $a < 0.1$ au must have migrated during the embedded Class 0/I phase (age $\tau \lesssim 2$ Myr) while there was still dissipative gas in the surrounding disk and envelope.

The physics of core and disc fragmentation set the initial masses of binary components. The seed components subsequently grow into stars by accretion. Components of wide binaries that form via core fragmentation tend to accrete from their respective gas reservoirs and form their own circumstellar disks (Bate et al. 1995; White & Ghez 2001; Offner et al. 2010; Bate 2014). Meanwhile, closer proto-binaries that derive from disk fragmentation clear out an inner cavity and subsequently accrete from a circumbinary disk (Artymowicz 1983; Artymowicz et al. 1991; Kratter & Matzner 2006; Clarke 2009). Accretion of gas onto a binary modifies its orbital separation, eccentricity, mass ratio, and the orientations of stellar rotation axes (spins), a process sometimes referred to as eigen-evolution (Kroupa 1995). Therefore, statistics of close binaries are determined by their accretion-driven migration. Here we propose a simple mathematical model of disk fragmentation, accretion, and migration that matches qualitatively the joint statistics of periods and mass ratios of real close binaries.

Some close binaries may also derive from dissipative capture of seed protostars formed by core fragmentation as they initially fell to the common centre of gravity via dynamical friction with the surrounding gas, and then subsequently accreted and migrated further inward within a circumbinary disk (Offner et al. 2010; Bate 2019), see also (Lee et al., submitted). This channel might be more relevant for close M-dwarf binaries where disk fragmentation is less likely (Kratter et al. 2010; Offner et al. 2010). For solar-type systems, however, there is strong observational evidence that a significant majority of companions within $a < 10$ au derived from disk fragmentation and migration. As already indicated, ≈90% of compact solar-type triples with $a_{\rm out} < 10$ au have small mutual inclinations $i_{\rm mut} < 40^\circ$ (Borkovits et al. 2016). Perhaps more compelling is the dependence on metallicity: the close binary fraction of solar-type stars ($a < 10$ au) is strongly anti-correlated with metallicity because optically thick disks become cooler and more prone to fragmentation with decreasing metallicity, but the wide binary fraction ($a > 200$ au) is independent of metallicity because fragmentation of optically thin cores is metallicity invariant (Badenes et al. 2018; Moe et al. 2019; El-Badry & Rix 2019). Quantitatively, Moe et al. (2019) measured the binary fraction within $a < 10$ au to decrease by a factor of ≈4 across $-1.0 <$ [Fe/H] < 0.5, but found the underlying separation distribution across $a = 0.1$ - 10 au to be insensitive to metallicity. El-Badry & Rix (2019) confirmed the emergence of a metallicity dependence within $a < 200$ au, demonstrating the fraction of solar-type primaries with $a \approx 50$ au companions decreases by a factor of ≈3 across $-1.0 <$ [Fe/H] < 0.5. The observations suggest $\gtrsim$90%, ≈70%, and $\lesssim$10% of solar-type binaries with $a < 10$ au, $a \approx 50$ au, and $a > 200$ au, respectively, derived from disk fragmentation. In any case, our model proposed here is applicable as long as the seed binary accretes most of its mass from a common circumbinary gas reservoir. For simplicity, we discuss only close solar-type and early-type binaries with $a < 10$ au that most likely formed via disk fragmentation.

The complexity and inherently stochastic nature of binary star formation have severely limited comparison of predictive models of binary statistics with observations. State-of-the-art hydrodynamical simulations of a dense collapsing cluster by Bate (2019, and earlier versions) nicely demonstrate this complexity by generating a population of binaries and triples resembling real systems in many ways. However, the limited number of objects formed in these closed-box simulations precludes detailed statistical comparison with observations, especially for relatively rare but astrophysically important massive OB stars. Moreover, the spatial resolution of these simulations is too coarse for producing close binaries with separations less than a few au. Finally, not all stars are born in such a dense cluster; formation of stars and stellar systems depends on the environment.

Section 2 discusses formation of binaries by disk fragmentation, their accretion-driven evolution, and the toy model of these processes developed here. Resulting statistics of simulated populations of solar-type and B-type binaries are presented in Section 3. The paper closes by a short discussion of the results in Section 4.

2 TOY MODEL OF BINARY FORMATION

The toy model presented here hides the complexity of close-binary formation behind simple prescriptions with random parameters. Our intent is to capture the essential aspects of this process and to reach a qualitative agreement with the observed statistics of periods P and mass ratios q of close binaries. The model does not explicitly consider eccentricity, spin vectors, or mutual inclinations between binary orbits and discs, but instead simply averages across these quantities. We simulate companions that derive from fragmentation, accretion, and migration in the disk, and so ignore companions that form beyond $a \gtrsim 3{,}000$ au via turbulent fragmentation of molecular cores. We also simulate triples, for which we model the fragmentation, accretion, and migration of the inner binaries and outer tertiaries independently. We present our baseline model parameters for solar-type and early-B primaries in Table 1, and we explore different parameter ranges in our supplementary models (Section 3.4). We adjust the parameters of our baseline model to mimic the real binary statistics, at least qualitatively (one cannot expect a perfect match from our crude model). Most importantly, by simulating large populations of multiple stars using a model with only a few free parameters, we can directly investigate how certain physical processes affect the properties of close binaries, e.g., how weighting disk fragmentation toward earlier or later times changes the mass-

ratio distribution, or how angular momentum transfer from the circumbinary disk to binary components alter the degree of correlation between periods and mass ratios.

2.1 Initial Conditions

Each system starts as a single star of seed mass $m_0 = 0.1 M_{\rm tot}$, where $M_{\rm tot}$ will be the final total mass of the system, e.g., M_1 for single stars, M_1+M_2 for binaries, and M_1+M_2+M_3 for triples. We explore different primary seed masses of $m_0 = 0.05 M_{\rm tot}$ and $0.15 M_{\rm tot}$ in models `PrimSeed1` and `PrimSeed2`, respectively. Multiplicity statistics are typically measured from observations across a narrow range of primary masses M_1 =[$M_{1,\rm low}$,$M_{1,\rm high}$], not system masses. We consider solar-type systems to span $M_1 = 0.7$ - $1.3\,\mathcal{M}_\odot$ while early-B primaries have $M_1 = 10$ - $20\,\mathcal{M}_\odot$. To encompass all possible combinations, we select the total final mass uniformly across $M_{\rm tot}$ = [$M_{1,\rm low}$,3$M_{1,\rm high}$]. Some simulated primaries will accrete above $M_1 > M_{1,\rm high}$, depending on the fragmentation and accretion evolution of the system. For each model, we remove such systems with massive primaries and simulate until there are $N_{\rm prim} = 10^3$ (or more) systems with final primary masses across M_1 =[$M_{1,\rm low}$,$M_{1,\rm high}$]. We keep track of the total number $N_{\rm tot} > N_{\rm prim}$ of systems actually simulated per model.

Protostellar accretion is a highly stochastic process. Infalling streams of gas are likely episodic. Moreover, protostellar disks experience recurrent thermal instabilities, which are manifested as FU Orionis outbursts. Hartmann & Kenyon (1996) estimated that young low-mass protostars undergo ∼20 FU Orionis outbursts during their initial ∼1-2 Myr. Discs tend to fragment when their gas temperatures become too cool and/or their accretion rates becomes too high so as to drive a gravitational instability according to the Toomre Q criterion (Kratter & Matzner 2006; Kratter et al. 2008; Machida et al. 2009; Tanaka & Omukai 2014; Kratter & Lodato 2016; Moe et al. 2019). Episodic accretion is therefore essential for disk fragmentation in two ways. First, the accretion rate during a burst is much larger than its average value, promoting instability and fragmentation. Second, the accretion energy is radiated away between the bursts, and therefore the disc temperature remains low before the subsequent burst. The infalling gas may not even settle into a viscous-supported disc but rather fragment almost immediately, as in the simulations by Goodwin et al. (2004). Kratter et al. (2008), Tanaka & Omukai (2014), and Moe et al. (2019) all found that discs of solar-type stars at solar metallicity are unlikely to fragment if they accrete constantly at their average rate of $\dot{M} \approx 10^{-6} \mathcal{M}_\odot\,{\rm yr}^{-1}$. Moe et al. (2019) emphasized that variability in the accretion rate is required; stochastic excursions up to $\dot{M} \approx 10^{-5} \mathcal{M}_\odot\,{\rm yr}^{-1}$, i.e., ∼10 times the average accretion rate, were sufficient to fragment the disc (see their Fig. 20). In our toy model, mass accretion occurs in $K_{\rm step}$ discrete episodes or intervals, with the mass $\Delta m = (M_{\rm tot} - m_0)/K_{\rm step}$ accreted in each episode. For our baseline model, we adopt $K_{\rm step} = 20$ and 50 for solar-type and early-B systems, respectively. We explore half and double these values in models `Step1` and `Step2`, respectively. At each accretion episode, a companion can form with a certain probability (see below). Physical time is not involved in our model, and by "time" $t = m/M_{\rm tot}$ we refer to the fraction of accreted mass.

Class II and even class I T Tauri disks, which have masses $M_{\rm disk} \sim 0.01\,M_1$ and $\sim 0.1\,M_1$, respectively (Sheehan & Eisner 2014; Ansdell et al. 2016; Sheehan & Eisner 2017), are unlikely to fragment due their small disc masses and low accretion rates (Kratter & Lodato 2016). As discussed in Section 1, disc fragmentation and accretion must have occurred in large part within the initial $\tau < 2$ Myr because the close binary properties of T Tauri stars match the field values (Kounkel et al. 2019).

The average frequency of companions formed during the mass buildup is determined by the free parameter $f_{\rm bin}$. We emphasize $f_{\rm bin}$ is not the final frequency of companions per primary. Some binaries may merge as they migrate within the Roche limit, and some triples may become disrupted as the outer tertiary migrates within the stability limit. Moreover, because we remove the systems with final $M_1 > M_{1,\rm high}$, the selected subset with M_1 =[$M_{1,\rm low}$, $M_{1,\rm high}$] have different multiplicity statistics than the simulated population as a whole. In our baseline model, we find $f_{\rm bin} = 0.3$ and 2.0 approximately reproduce the multiplicity statistics of solar-type and early-B primaries, respectively. In the supplementary models `Mult1` and `Mult2` the companion frequency is decreased or increased.

In our baseline model, we assume fragmentation occurs with equal probability across all accretion episodes. E.g., for our baseline solar-type model, there are 20 accretion episodes, each of which has a $f_{\rm bin}/20 \approx 1.5\%$ chance of forming a new companion. The accretion rates and stochastic variability of embedded Class 0 protostars are higher than their older Class I counterparts (Froebrich et al. 2006; Krumholz et al. 2009; Peters et al. 2010; Dunham et al. 2014; Hartmann et al. 2016), and so fragmentation may preferentially occur during earlier episodes. To encompass this possibility, we consider a model `Frag1` in which the probability of fragmentation is $p \propto t^{-0.5}$, i.e., the first accretion episode at $t = 0.1$ is three times more likely to form a new companion than the last episode. Alternatively, the accretion rate may initially increase with time or it may take several episodes for the disk to increase in mass and radius (McKee & Tan 2003; Girichidis et al. 2012), and so disk fragmentation may not occur until later times (see Fig. 5 in Kratter et al. 2008). We therefore also consider a model `Frag2` with $p \propto t^{0.5}$ so that the likelihood of disk fragmentation is weighted toward later episodes.

Disc instabilities are stochastic and therefore can be recurrent, i.e., some discs can experience two fragmentation episodes to produce triples. In our baseline model, two fragmentation events can occur within two successive episodes. It may actually take a finite interval for the disk to recover from the initial gravitational instability, increase in mass, and become prone to fragmentation again. Nonetheless, the compact coplanar triple protostar investigated by Tobin et al. (2016) is a case example where the first companion has migrated only slightly inward to $a \approx 60$ au while the outer tertiary at $a \approx 180$ au (marginally stable) has only recently fragmented from the disk.

Models of gravitational disk instability suggest the initial fragment mass is $M_{\rm frag} \approx \epsilon \Sigma \lambda^2$, where Σ is the disk surface density, $\lambda = 2\pi H$ is the most unstable wavelength given the scale height H of the disc, and $\epsilon \approx 0.5$ is a constant (Goodman & Tan 2004; Kratter et al. 2008; Boley et al. 2010; Kratter & Lodato 2016; Tobin et al. 2016). This corresponds

Table 1. Parameters of our baseline model.

Parameter	Description	Solar-type	B-type
$M_{\rm tot,0}$, $M_{\rm tot,1}$	Primary mass range, $\mathcal{M}_\odot$	[0.7, 1.3]	[10, 20]
$K_{\rm step}$	Number of accretion episodes	20	50
$f_{\rm bin}$	Average number of companions	0.3	2.0
$f_{\rm m0}$	Initial primary mass $m_0 = f_{m0}M_{\rm tot}$	0.1	0.1
f_{20}	Initial companion mass, fraction of $m_{\rm acc}$	0.25	0.25
$f_{\rm m2max}$	Maximum companion growth in one episode	1.0	1.0
a_0, a_1	Initial separations, au	[40, 1000]	[40, 3000]
β	Parametrization of the q-dependence	0.7	0.7
η_0, η_1	Range of migration coefficient η	[0, 3]	[0, 4]

to $M_{\rm frag} \approx 0.01\ \mathcal{M}_\odot$ and 0.1 $\mathcal{M}_\odot$ for representative unstable disks of solar-type and early-type primaries, respectively. For our baseline model, we adopt initial companion masses of $f_{\rm m20} = 0.25$ fraction of mass accreted in each episode. For solar-type and B-type stars these masses are typically 0.0125 and 0.075 $\mathcal{M}_\odot$, respectively; they are proportional to $M_{\rm tot}$. We consider half and double these companion seed masses in models `CompSeed1` and `CompSeed2`, respectively. These studies also show that the initial fragment inevitably accretes and clears a gap in the disk, roughly doubling in mass. In our model, the companion growth in each accretion episode is restricted to a fraction $f_{\rm m2max} = 1$ of its current mass (no more than double). This restriction is relevant only for the first episodes, when the companion has a small mass. We also consider supplementary models `MaxAcc1` and `MaxAcc2` where the growth parameter is decreased and increased by a factor of two.

We select the initial separation of the companions from a log-uniform distribution across the interval $a_0 = [a_{\rm min}, a_{\rm max}]$. For disks with solar-metallicity opacities, Moe et al. (2019) showed that the gas cooling timescales at separations below $r < 40$ au are too long to achieve fragmentation. We therefore adopt a minimum initial separation for disk fragmentation of $a_{\rm min} = 40$ au in all our models. Ansdell et al. (2016, 2018) utilized ALMA observations of CO molecular transitions to measure the gas disk radii and masses of dozens of low-mass protostars in Lupus (≈1-3Myr). They found the gas radii span $r \approx$ 70-500 au, larger than that inferred from continuum dust emission, but with gas masses that are currently only ≈ 0.2 - 3 $M_{\rm J}$. Gravitational instability requires younger, more massive disks ($M_{\rm disk}/M_* > 0.1$; Kratter & Lodato 2016), which are expected to be even larger. Indeed, despite their short lifetimes and propensity for instability, there are a handful of massive disks with $M_{\rm disk}/M_* \sim 0.1$ - 1.0 around early-B protostars with $M_* \sim 5$ - 20 $\mathcal{M}_\odot$ that extend to $r \approx$500 - 2,000 au (Cesaroni et al. 2007, references therein). In our baseline model, we set the maximum separation for disk fragmentation to be $a_{\rm max}$ = 1,000 au and 3,000 au for solar-type and early-B primaries, respectively. In our model, the accretion-induced migration does not depend on the absolute value of the separation, hence the final distribution of separations and periods is a simple convolution of the initial distribution of $\log a$ with the distribution of the migration factor $\log(a_{\rm final}/a_{\rm init})$. The choice of initial separations is almost irrelevant, if we neglect mergers. Given the log-uniform separation distribution across $a_0 = [a_{\rm min}, a_{\rm max}]$, the median disk fragmentation separation is 200 au and 350 au for solar-type and early-B systems, respectively, in our baseline model.

2.2 Binary Accretion

Evolution of accreting binaries has been studied by many authors over the past three decades (e.g. Artymowicz & Lubow 1996; Bate & Bonnell 1997). The infalling gas accumulates near the inner edge of the circumbinary disk, falls onto the binary through fast streams (or arms), and temporarily settles into circumstellar disks around each component before being accreted by them. The lower-mass companion is closer to the edge of the circumbinary disk and sweeps out a larger area in its Keplerian orbit. For a binary in a circular orbit that accretes cold gas from a coplanar circumbinary disk, it is generally accepted that most of the accreted mass is directed toward the companion (Bate & Bonnell 1997; Farris et al. 2014; Young & Clarke 2015).

Let f_2 be the mass fraction accreted by the secondary: $\mathrm{d}M_2 = f_2 \mathrm{d}m$ and $\mathrm{d}M_1 = (1 - f_2)\mathrm{d}m$. By definition, $f_2 = 0.5$ when the mass ratio $q = M_2/M_1 = 1$ is unity. For cold gas, i.e., negligible sound speed relative to Keplerian orbital velocity ($c = c_{\rm s}/\sqrt{GM/a} \approx 0.1$), Farris et al. (2014) established $f_2 = 1/(1 + q)$ based on a suite of 2D hydrodynamic simulations. The secondary grows preferentially until the components become comparable in mass. Young & Clarke (2015) explored accreting binaries with different mass ratios and gas temperatures. They found a similar but slightly different relation $f_2 = q/(1 + q)$ for accretion of cold gas with $c = 0.05$. For hotter gas with $c = 0.25$, they showed the respective accretion rates were less sensitive to the mass ratio, e.g., $f_2 \approx 0.65$ for $q = 0.1$. For young protobinaries that have recently formed, i.e., high accretion rates and initially wide separations $a \sim 100$ au ($v_{\rm orb} \sim 3$ km s^{-1}), the infalling gas is likely to accrete somewhere between these cold or hot regimes. Specifically, such massive discs prone to fragmentation have mid-plane temperatures $T \approx$ 20 - 80 K near $r \sim 100$ au (Boss 1998; Kamp & van Zadelhoff 2001; Kamp & Dullemond 2004; Kratter & Matzner 2006; Kratter et al. 2008; Williams & Cieza 2011), yielding thermal velocities $c_{\rm s} \approx$ 0.3 - 0.6 km s^{-1} and therefore intermediate values of $c = c_{\rm s}/v_{\rm orb} \approx$0.1 - 0.2. Hanawa et al. (2010) and de Val-Borro et al. (2011) investigated the accretion of hot gas ($c \approx 0.2$) onto binaries with $q > 0.7$. Spiral density patterns developed in their circumbinary discs, which caused the accretion rates onto the circumprimary and circumsecondary discs to vary with a slight preference toward the former, i.e., $f_2 \approx$ 0.4 - 0.5. Zhao & Li (2013) included the effects of

magnetized cores in their MHD simulations, and found the binary was fed by a collapsing pseudo-disk instead of typical circumstellar and circumbinary disks, and that the more massive primary preferentially accretes more of the gas. Finally, Dunhill et al. (2015) showed that an eccentric binary with $e = 0.6$ precesses relative to the disk, resulting in an oscillating f_2 that averages to ≈ 0.5 after many precession timescales.

Infalling material onto the disk does not necessarily have the same angular momentum direction as the disk, and so each accretion episode can torque and warp the disk relative to the plane of the binary orbit. Although very close T Tauri binaries with $a < 1$ au tend to have coplanar prograde disks, the disks around wider T Tauri binaries with $a = 1$ - 100 au exhibit a wide distribution of mutual inclinations from coplanar prograde to orthogonal (Czekala et al. 2019). Misaligned disks may tear apart into multiple rings, causing chaotic accretion onto the binary components (Nixon et al. 2013; Doğan et al. 2015). Hydrodynamic simulations show that the orbit-averaged accretion rates onto the primary and secondary are more comparable when the disk is misaligned or retrograde (Hayasaki et al. 2013; Ivanov et al. 2015).

All the hydrodynamic simulations considered above incorporate sink particles for the binary components such that all the mass in the circumprimary and circumsecondary disks are eventually accreted by the primaries and secondaries, respectively. In reality, mass is never completely conserved. Young stellar objects lose mass and angular momenta via disk accretion winds, outflows, and jets (see reviews by Frank et al. 2014; Bally 2016; Hartmann et al. 2016). For T Tauri stars, the measured disk mass loss rates are roughly a few percent of and linearly proportional to the mass accretion rates (Hartigan et al. 1995; Rigliaco et al. 2013; Natta et al. 2014). However, younger class 0/I protostars tend to exhibit collimated Herbig-Haro jets (Reipurth & Bally 2001; Bally 2016), and are expected to have substantially lower accretion efficiencies (Behrend & Maeder 2001; Haemmerlé et al. 2016, 2019). To match the observed birthlines of intermediate-mass pre-MS stars on the HR diagram, Behrend & Maeder (2001) found that protostars accrete only ≈30% of the mass from the disk. Toward high accretion rates and more massive protostars, perhaps only ≈10% of the mass in the disk is accreted (Haemmerlé et al. 2016).

We predict that the accretion efficiencies will be even smaller in very young proto-binaries. Consider a $0.3\mathcal{M}_\odot$ primary accreting from a marginally unstable disk, i.e. $\approx 10^{-5}$ $\mathcal{M}_\odot$ yr^{-1} to achieve gravitational instability. The disk fragments and forms a new companion that accretes to $\approx 0.03\mathcal{M}_\odot$ as it clears a gap and inner cavity. At this time when $q = 0.1$, most of the mass is initially directed toward the secondary, but the secondary can only accrete and retain material on its thermal Kelvin-Helmholtz timescale $\dot{M}_{\rm KH} = RL/GM \sim 10^{-7}$ $\mathcal{M}_\odot$ yr^{-1} (Kippenhahn & Meyer-Hofmeister 1977; Pols & Marinus 1994). In response to the high accretion rate, the secondary expands while the excess mass builds up in the circumsecondary disk. If the high accretion rate is sustained, then not even the circumsecondary disk can retain the excess material, which is either lost via polar outflows and jets, draining angular momentum from the system, or re-directed toward the circumprimary disk. In any case, when the protobinary initially forms, i.e., in the high accretion rate regime and $q \lesssim 0.1$, most of the mass is lost from the system and f_2 is lower than in the ideal conservative scenario. The parameter $f_{\rm m2max}$ is introduced in the model to limit the growth of low-mass companions. In our baseline model, we set $f_{\rm m2max} = 1$, i.e., the secondary can at most double during a single accretion episode.

In our toy model, we adopt the following parameterization for the mass fraction accreted by the secondary:

$$f_2 = \Delta M_2/\Delta M = 0.5 + 0.5x(1-q)^\beta, \quad (1)$$

where $\beta = 0.7$ in our baseline model and $x = [0,1]$ is a uniformly distributed random number uniquely generated for each accretion episode. We consider $\beta = 0.5$ and 0.9 in models `Beta1` and `Beta2`, respectively. Note that $x = 1$ represents the ideal scenario of cold gas, circular orbits, prograde coplanar discs, no magnetic fields, and mass conservation. Any departure from these five criteria cause $x < 1$, and in our toy model a uniform random variable $x = [0, 1]$ for each accretion episode accounts for these various physical processes.

2.3 Binary Migration

The response of the binary separation to the portion of accreted gas depends on the specific angular momentum and angle of the infalling gas with respect to the binary orbit along with other factors, e.g., angular momentum losses via disk outflows and jets. The evolution of the binary's separation should be proportional to the relative mass accreted by the secondary component,

$$\frac{{\rm d}a}{a} = -\eta\frac{{\rm d}M_2}{M_2}, \quad (2)$$

where the parameter η defines the speed and direction of migration (see e.g. eq. 6 in Roedig & Sesana 2014). In some works, the migration coefficient η is defined in relation to the total mass increment ${\rm d}m/m$. Both definitions are equivalent at large mass ratios q, but at small q the relative mass increment of the companion, not of the total mass, is the relevant parameter for migration.

Assuming the gas is co-moving with the binary, i.e., the gas and binary orbit have the same specific angular momentum, then accretion by the binary causes the orbit to shrink according to $a \propto M^{-1}$, i.e., $\eta = 1$ (Bonnell & Bate 2005; Umbreit et al. 2005). These studies also showed that if the gas is at rest with respect to the binary, then the total angular momentum L of the binary orbit must be conserved, leading to $a \propto M^{-3}$, i.e., $\eta = 3$. Umbreit et al. (2005) also examined counter-rotating gas with respect to the orbit, and found even stronger inward migration, i.e., $\eta = 5$. Bonnell & Bate (2005) considered a random-walk evolution, whereby the angular momentum of each infalling gas parcel is randomly oriented with respect to the binary. In this scenario, they showed analytically $a \propto M^{-2}$, i.e., $\eta = 2$, confirmed by their numerical simulations. Finally, Goicovic et al. (2017) used a 3D SPH code to simulate rapid accretion (within 4–8 binary periods), and measured $\eta = 3.45$ for prograde gas, $\eta = 5.6$ for random orientation, and $\eta = 7.4$ for retrograde gas. The random-walk or rapid-accretion scenarios likely apply to wide binaries. E.g., nascent cores at initial $a \approx 5{,}000$ au with ∼10% their final mass will migrate to $a \approx 50$ au according to the random-walk hypothesis. Even without accretion, wide binaries can migrate significantly inward via

dynamical friction (Offner et al. 2010; Bate 2019) (Lee et al., submitted).

At closer separations, however, binaries likely accrete from a circumbinary disk, which has a specific angular momentum larger than the binary's. Bate & Bonnell (1997) showed that a binary that accretes prograde and aligned gas will expand, i.e., $\eta < 0$. Utilizing a 2D grid code, Tang et al. (2017) explored whether the binary expands or shrinks as it accretes from a coplanar circumbinary disk. The answer depends on the the size of the circirumstellar disks, parameterized by the sink time τ_s in units of the binary period. For a fast sink ($\tau_s \ll 1$), the disks are small, the overall torque is positive, and the binary expands. Conversely, for slow sinks ($\tau_s = 5$), Tang et al. (2017) showed the binary shrinks according to Eqn. 2 with $\eta = 3.16$. The gas streams arriving at the components are accelerated and repelled back to the cavity edge, and this "gravitational slingshot" mechanism brakes the binary. Muñoz et al. (2019) also performed 2D simulations of accretion from a circumbinary disk with higher resolution and over longer (viscous) timescales until a steady-state was reached. They always found orbital expansion, i.e., $\eta = -2.15$ for a circular orbit and $\eta = -0.47$ for $e = 0.6$.

There are three important caveats that would counteract the expectation from 2D hydrodynamic simulations that binaries expand as they accrete from a circumbinary disk. First, the majority of T Tauri binaries with $a = 1$ - 100 au accrete from misaligned disks (Czekala et al. 2019). Although not a true random-walk scenario with $\eta = 2$, the discs may be sufficiently misaligned so as to result in inward migration with $\eta > 0$. Second, the cores and disks are likely magnetized, and MHD simulations have shown that accretion of magnetically-braked material substantially shrinks the separation of the binary (Zhao & Li 2013). Finally and most important, the numerical simulations assume mass conservation, but as discussed above, most of the mass in the disks, especially the circumsecondary disk, are lost via outflows and jets, draining angular momentum from the system.

In our toy model, we therefore consider a variable η, unique for each accretion episode, and with a positive average $\langle\eta\rangle > 0$, i.e., net inward migration. Eqn. 2 applies only in the limit where $dM_2 << M_2$. We adopt a more general form:

$$a = a_0 \exp(-\eta \Delta M_2/M_2), \quad (3)$$

where ΔM_2 is the mass accreted by the secondary in each accretion episode. We find a uniform random variable $\eta = [0, 3]$ adequately reproduces the observations and accounts for the three factors indicated above, i.e., misaligned disks, magnetic fields, and mass loss. We consider different ranges of η values in supplementary models `Eta1` and `Eta2`, respectively. In the first accretion episodes when the companion's growth is limited by the parameter $f_{\rm m2max}$, we evaluate Eqn. 3 at the full, unlimited ΔM_2 according to Eqn. 1 to account for the angular momentum losses and impact on the binary orbit, even though the secondary actually retains no more than $f_{\rm m2max} M_2$ mass.

A migrating binary may become too close and merge if the stars overfill their Roche lobes. The merging condition is approximately $a < 2.5R$ (Eggleton 1983), where the primary radius R is estimated from the primary mass according to $R/R_\odot = 1.5(M_1/\mathcal{M}_\odot)^{0.8}$, as appropriate for pre-MS stars. Similarly, tertiary companions may migrate within three times the separation of the inner binary, becoming dynamically unstable. In our baseline model, we eject such tertiaries (the ejected mass is lost). In supplementary model `Fold1`, we dynamically unfold such unstable configurations by increasing the outer separation by a factor from 100 to 1000, compared to its current (unstable) separation. The unfolding factor has a log-uniform distribution. At the same, time, we shrink the inner semimajor axis by a factor of two at each unfolding.

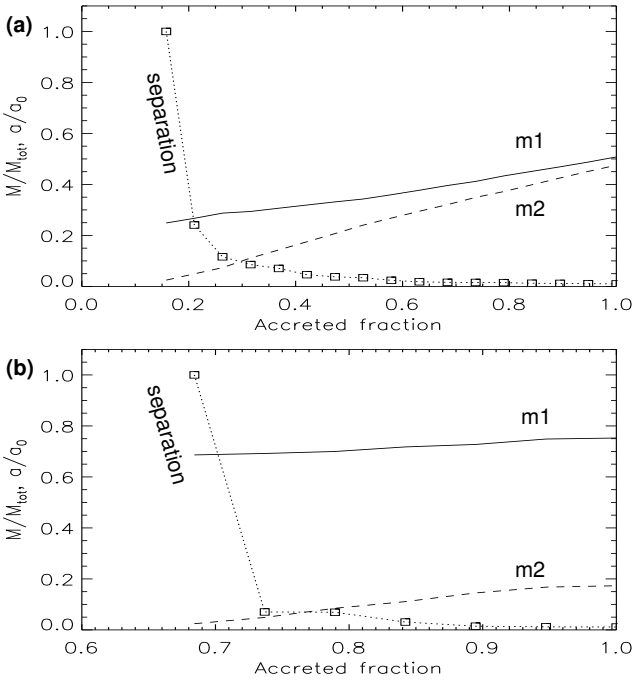

Figure 1. Evolution of two simulated solar-type binary systems. The full and dashed lines show the fraction of the primary and secondary mass, respectively, as a function of the total accreted mass. The squares connected by dotted line show the evolution of the semimajor axis, also in relative units. In the first binary (a), the companion formed when 0.15 of the total mass was accreted and had a chance to become almost equal to the primary, while the separation decreased by a factor of 100. The second example (b) shows companion formation at time 0.65. In both cases, migration is strongest right after the companion formation, when its mass is still small.

2.4 Summary of the toy model

The toy model generates large samples of simulated binaries by implementing the physically-motivated prescriptions discussed above in a simple numerical code. Here its operation is summarized. The baseline parameters of the model for solar-type and B-type stars are listed in Table 1.

For each simulated system, the total mass $M_{\rm tot}$, uniformly distributed between $M_{\rm tot,0}$ and $3M_{\rm tot,1}$, is generated. This defines the initial mass of the primary star, $f_{m0} M_{\rm tot}$, and the mass accreted in each episode, $m_{\rm acc} = M_{\rm tot}/K_{\rm step}$. The mass is added to the primary star until a companion with the initial (seed) mass of $f_{\rm m2} m_{\rm acc}$ is formed. The prob-

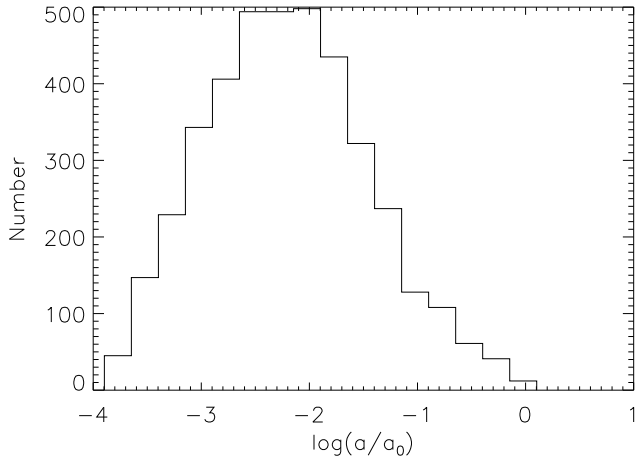

Figure 2. Distribution of the orbital migration factor $\log(a/a_0)$ for solar-type stars.

ability of companion formation in each episode is $f_{\rm bin}/K_{\rm step}$, and its initial separation is chosen from a log-uniform distribution in the interval $[a_0, a_1]$. Formation of additional companions in subsequent accretion episodes is not prohibited, but only dynamically stable outcomes are allowed (companion separation more than three times larger than the separation of the inner binary).

The evolution of a system (single, binary, triple, etc.) in response to the an accretion episode is implemented as a subroutine. The accreted mass $m_{\rm acc}$ is distributed between components according to the Eqn. 1 using the parameter β and a uniformly distributed random number x, generated independently for each episode. The growth of the companion is restricted by the parameter $f_{\rm m2max}$. Then Eqn. 3 is applied, with a random η uniformly distributed between η_1 and η_2, independently in each episode. Using the updated separation, we check the merging condition (if satisfied, the binary becomes again a single star with the sum of component's masses). If the number of components exceeds two, the evolution subroutine is called recursively (with independent random numbers), and the condition for dynamical stability is checked to eliminate (or unfold) unstable triples. Figure 1 illustrates evolution of two typical solar-mass binaries.

When all mass is accreted by the system in $K_{\rm step}$ episodes, we consider only single stars, binaries, and higher-order hierarchies with primary masses in the $M_{\rm tot,0}$, $M_{\rm tot,1}$ range. Single stars with these masses are simply counted. The counters of mergers and disruptions are incremented only for systems in the requested range of primary mass. Generation of systems is repeated until the total requested number of binaries is reached. Figure 2 shows the distribution of the ratio of final and initial semimajor axes $\log(a/a_0)$ (i.e. the migration factor) for solar type stars. The median is −2.2, meaning that the initial binary separation is reduced typically by two orders of magnitude. In the toy model, the distribution of final binary separations or periods is a simple convolution of the initial distribution (assumed log-uniform) with that of the migration factor.

The statistics of the simulated binary population is characterized by several parameters (Table 2). We consider

Table 2. Statistical parameters

Parameter	Description
CF	Companion fraction, $N_{\rm comp}/N_{\rm sys}$
BF	Fraction of pairs, $\log P < \log P_{\rm max}$
TF	Fraction of triples, $\log P_{\rm out} < \log P_{\rm max}$
$f_{\rm disrupt}$	Fraction of disrupted systems
$f_{\rm merge}$	Fraction of mergers
γ_q	Power-law of $f(q)$, $0.3 < q < 0.95$
$f_{\rm twin}$	Excess twin fraction among $q > 0.3$
γ_P	Slope of $N(\log P)$ in the (0.3, 2) interval

all pairs, independently of their hierarchy (both inner and outer subsystems in triples) and determine the total companion fraction CF accordingly. However, the binary and triple fractions, BF and TF, refer only to pairs with periods less than $P_{\rm max}$, chosen at 10^4 days for solar-type stars and $10^{3.4}$ days for B-type stars. Only short-period binaries can be generated by the toy model, so the resulting statistics are meaningful at separations below ∼10 au, motivating the choice of $P_{\rm max}$. The mass ratio distribution at $q > 0.3$ is characterized by the truncated power law with index γ_q and the excess twin fraction $f_{\rm twin}$ (fraction of binaries with $q > 0.95$ in excess of the power law, relative to all binaries with $q > 0.3$), as in Moe & Di Stefano (2017). We compute these parameters in two period intervals, $\log(P)$ (in days) of (0 - 2) and (2 - 4) for solar-type binaries, (0 - 1.7) and (1.7 - 3.4) for B-type binaries (with subscripts S and L, respectively). The period distribution $N(\log P)$ is fitted by a straight line in the $\log(P)$ interval (0.3 - 2), and its slope γ_P quantifies the overall migration. Strong migration of B-type binaries produces an excess of short periods, with a negative γ_P and a large rate of mergers. In contrast, for solar-type binaries the slope is positive and the number of mergers is very small.

3 RESULTS

We list the results of our simulations for solar-type and early-B binaries in Tables 3 and 4, respectively, for our baseline and all supplementary models. We also compare the simulated parameters to the observations according to the 67-pc sample of solar-type systems (Tokovinin 2014), meta-analysis of solar-type and early-type multiples (Moe & Di Stefano 2017), and other surveys as described below. Data of recent publications on these stars are used. The observed statistical parameters of binaries are given in the first lines of both Tables in italics.

3.1 Solar-mass binaries

In Fig. 3, we show the periods P and mass ratios q of individual companions to solar-type primaries in our baseline model. The thick line depicts the range of initial binary periods, corresponding to a_0 = 40 - 1,000 au. Binaries that formed early have, on average, migrated to shorter periods and have larger q. Various surveys have demonstrated that solar-type primaries exhibit a dearth of close brown dwarf companions within $P \lesssim 100$ days, commonly known as the brown dwarf desert, but that the frequency of brown dwarf

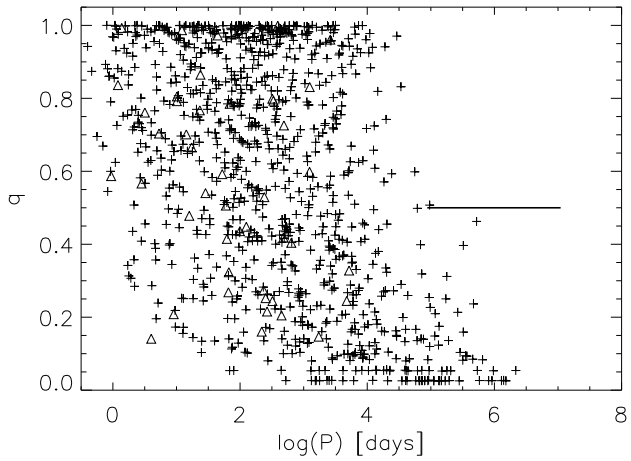

Figure 3. P, q plot of 1000 simulated solar-mass binaries. The horizontal line shows the range of initial periods. Binary, triple, and quadruple systems are plotted as pluses, triangles, and squares.

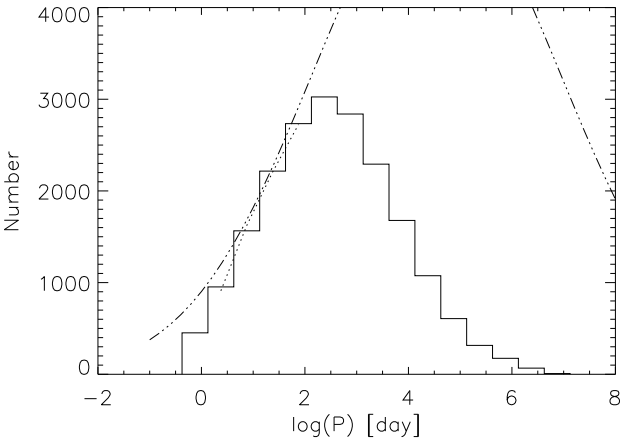

Figure 4. Period distribution of solar-type binaries. Full line — simulations, dash-dot line — Gaussian model, dotted line — power law.

companions increases with increasing separation (Grether & Lineweaver 2006; Kraus et al. 2008, 2011; Csizmadia et al. 2015; Wagner et al. 2019; Shahaf & Mazeh 2019). Our model naturally reproduces the brown dwarf desert, as it is very difficult for very low-mass companions to migrate within $P \lesssim 100$ days without also accreting above $M_2 > 0.08\,\mathcal{M}_\odot$. Meanwhile, we simulate many brown dwarfs at longer periods, which were companions that fragmented at late times and therefore accreted and migrated very little.

In the field, ≈20% of solar-type stars have MS companions within $a < 10$ au ($P < 10^4$ days; Moe & Di Stefano 2017; Moe et al. 2019). This fraction increases slightly to BF ≈ 22% after including the observed population of brown dwarf companions across $a = 1\text{-}10$ au. In the simulated sample, we get a slightly larger BF of 30%, but it is easily adjustable by reducing $f_{\rm bin}$.

The overall triple-star fraction of solar-type stars is ≈13%, but only 17 (≈0.3%) of the solar-type primaries in the 67-pc sample are in known compact triples with $a_{\rm out} < 10$ au (Tokovinin 2014). However, the observed compact triple star fraction is a lower limit due to incompleteness, as it is very difficult to detect faint low-mass tertiaries within $a_{\rm out} < 10$ au. Indeed, in our baseline model, the majority of compact triples have $q_3 = M_3/M_1 < 0.3$ (see Section 3.3). Brandt (2018) recently combined *Gaia* DR2 and *Hipparcos* astrometry to detect accelerating systems, indicative of binary companions with intermediate separations of $a \approx 1\text{-}50$ au. Of the 232 binaries with $P < 100$ days in the 67-pc sample, 31 exhibit statistically significant astrometric acceleration. These accelerations are, mostly, not caused by wide, easily resolvable tertiaries beyond $a_{\rm out} > 10$ au. Instead, the majority of the 31 close binaries exhibiting astrometric acceleration are likely previously unrecognized compact triples with $a_{\rm out} < 10$ au. Moreover, it is also challenging to identify compact A-Ba,Bb triples, e.g., a pair of low-mass M-dwarfs closely orbiting a solar-type primary, utilizing traditional methods of RV monitoring and high-contrast imaging. Nonetheless, examinations of *Kepler* eclipsing binaries exhibiting eclipse timing variations reveal a large population of compact A-Ba,Bb triples (Borkovits et al. 2016, references therein). Considering the selection biases, we estimate a compact triple star fraction of TF ≈ 1% for solar-type primaries, similar to our baseline model value of TF = 3%.

Although we selected $f_{\rm bin} = 0.3$ apriori to roughly match the observed close companion fraction, the *ratio* of compact triples to close binaries was not predetermined. We estimate TF/BF ≈ 1%/22% ≈ 5% for the observed sample of solar-type primaries, and compute TF/BF = 3%/30% ≈ 10% for our baseline model. By treating disc fragmentation as a stochastic repeatable process, our model qualitatively reproduces the observed ratio of compact triples to close binaries.

Both the observed and simulated solar-type binaries are weighted toward larger periods, as shown in Figure 4. In our baseline model, only 0.4% of solar-type primaries had merged with a very close binary companion ($\log P \lesssim -0.4$), and 4% of primaries have companions that migrated to $P = 1\text{-}10$ days. The latter value is comparable to 2% observed both in the field and in young star-forming regions (Moe & Kratter 2018). The field solar-type binary period distribution is roughly log-normal, peaking at $\log P = 4.8$ with dispersion of 2.3 dex (Duquennoy & Mayor 1991; Raghavan et al. 2010; Tokovinin 2014). Across $\log P = 0.3\text{-}2$, the observed slope is $\gamma_{\rm P} = {\rm d}N/{\rm dlog}P = 0.7$, consistent with the simulated value of $\gamma_{\rm P}$. However, at longer periods $\log P \gtrsim 2.5$, the simulated distribution flattens and turns over, underestimating the true frequency of companions at intermediate separations (Fig. 4).

We surmise that binaries which formed via core fragmentation, which are not included in our model, begin to contribute at a non-negligible level beyond $a \gtrsim 1$ au. Indeed, although the majority of double-double quadruples have been observed in loose hierarchies with $a_{\rm out} > 10$ au, a few have been detected in compact configurations with $a_{\rm out} = 1\text{-}10$ au (Tokovinin 2014). Such double-double quadruples cannot derive from successive inside-out disk fragmentation episodes as encapsulated by our model, but instead via an outside-in process whereby a wide binary first forms via core fragmentation and then both of those components subsequently split via disk fragmentation. The existence of com-

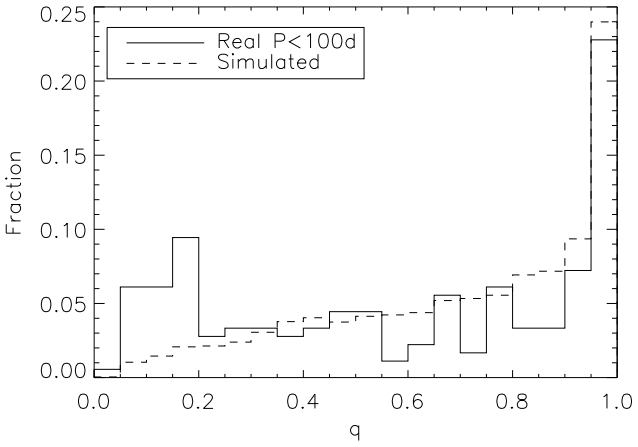

Figure 5. Distribution of the mass ratio q of solar-type binaries with $1 < P < 100$ days. Full line — binaries in the 67-pc sample (Tokovinin 2014), dashed line — simulations.

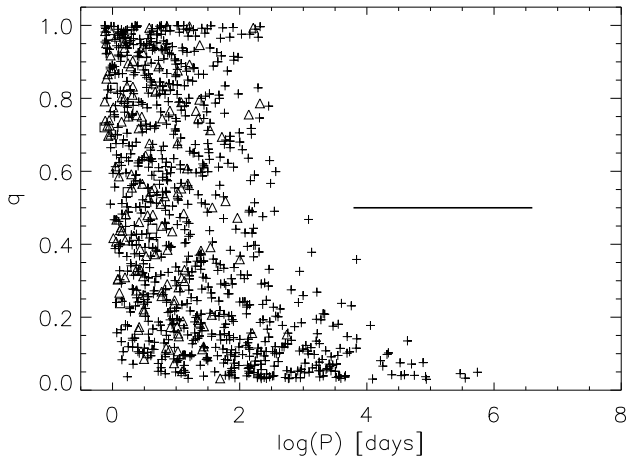

Figure 6. P, q plot of 1000 simulated B-type binaries. The horizontal line shows the range of initial periods. Binary, triple, and quadruple systems are plotted as pluses, triangles, and squares.

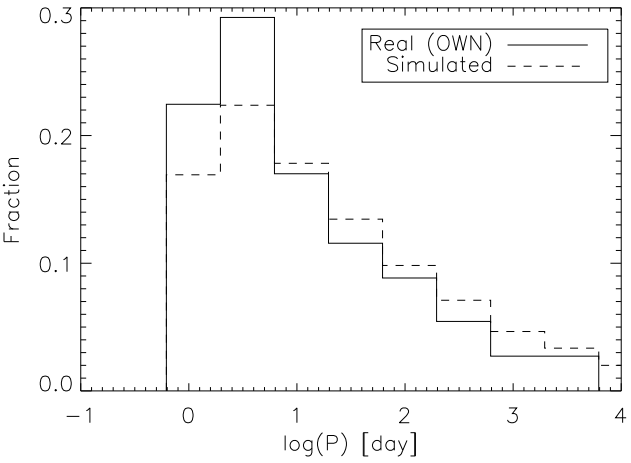

Figure 7. Histograms of periods for B-type binaries. The observed period distribution of massive binaries is taken from the OWN survey by Barbá et al. (2017).

pact double-double quadruples with $a_{\rm out} = 1$ - 10 au strongly suggests that binaries that formed via core fragmentation can migrate to such intermediate separations. Core fragmentation binaries become more relevant with increasing separation. The contribution from disk versus core fragmentation binaries are comparable near $a \approx 50$ au (see Introduction), the peak in the overall period distribution of solar-type binaries. Both Moe et al. (2019) and El-Badry & Rix (2019) showed that the fraction of wide binaries ($a > 200$ au; $P > 10^6$ days) is independent of metallicity, and so they concluded nearly all such wide binaries are the result of core fragmentation. As shown in Fig. 4, our model population of disk fragmentation binaries steadily declines to zero near $\log P = 6$, consistent with the observational constraints.

Our model also reproduces the observed excess fraction of twins with $q > 0.95$, especially evident at short periods. In Figure 5, we compare the simulated mass-ratio distribution of solar-type binaries with $P = 1$ - 100 days to the observed distribution in the 67-pc sample (Tokovinin 2014) across the same period range. For the latter, we use the measured mass ratios of double-lined spectroscopic binaries (SB2s) and the minimum mass ratios of SB1s. Across the interval $q = 0.3$ - 1.0, the observed and simulated mass-ratio distributions are well described by a power-law with slope $\gamma_{q,S} \approx 1$ and an excess twin fraction $f_{\rm twin,S} \approx 0.2$ relative to the power-law component. However, Moe & Di Stefano (2017) noted that a non-negligible fraction of solar-type SB1s with small q in the field contain white dwarf companions, and so the intrinsic distribution of close MS companions are further weighted toward higher q. Accounting for this bias, we estimate $\gamma_{q,S} = 0.8$ and $f_{\rm twin,S} = 0.24$ in the field. Fitting the simulated sample of solar-type binaries with $P = 1$ - 100 days yields $\gamma_{q,S} = 1.5$ and $f_{\rm twin,S} = 0.20$, qualitatively consistent with the observations.

With increasing period, the mass-ratio distribution becomes weighted toward smaller values. In our simulations, the power-law slope decreases from $\gamma_{q,S} = 1.5$ to $\gamma_{q,L} = 0.2$ from $\log P$ (days) = 0 - 2 to 2 - 4, and the excess twin fraction also decreases from $f_{\rm twin,S} = 0.20$ to $f_{\rm twin,L} = 0.15$. There is strong observational evidence that the solar-type excess twin fraction decreases across $\log P = 0$ - 4 (Lucy & Ricco 1979; Tokovinin 2000; Moe & Di Stefano 2017). Utilizing the 25-pc (Raghavan et al. 2010) sample of solar-type primaries, Moe & Di Stefano (2017) measured the excess twin fraction to decrease linearly with $\log P$ such that $f_{\rm twin,L}/f_{\rm twin,S} \approx 0.7$, consistent with the simulated ratio $f_{\rm twin,L}/f_{\rm twin,S} \approx 0.75$.

3.2 Massive binaries

Massive stars form by accreting more matter than solar-type stars. We set a larger number of accretion bursts $K_{\rm step} = 50$ accordingly, as well as a larger probability of forming a companion. Figures 6 shows the results for B-type binaries. For volume-limited samples, ≈50% of early-B stars have companions within $a < 10$ au ($\log P \lesssim 3.2$), and ≈10% of early-B primaries are in compact triples with $a_{\rm out} < 10$ au (Moe & Di Stefano 2017). In our baseline early-B model with $f_{\rm bin} = 2.0$, we simulate BF = 0.56 and TF = 0.13, respectively,

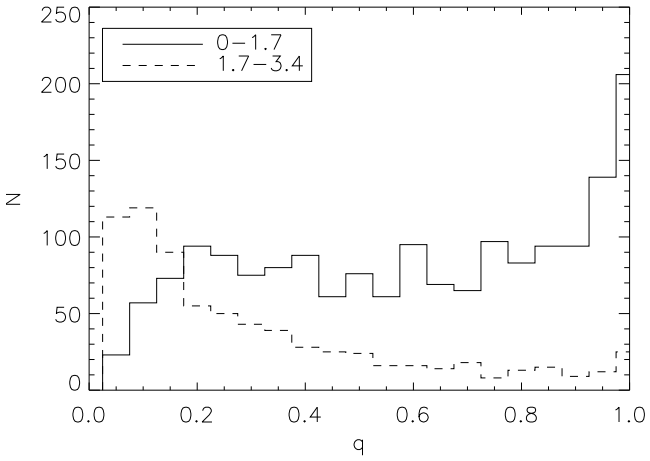

Figure 8. Histogram of the mass ratio of simulated B-type binaries in period intervals log(P) of 0-1.7 and 1.7-3.4.

close to the observations. The simulated ratio of compact triples to close binaries, TF/BF ≈ 0.2, is higher for early-B systems, consistent with the observations. In our model, disk fragmentation is a Poisson process, and so increasing the mean number of companions $f_{\rm bin}$ not only increases the ratio of close binaries to single stars but also the ratio of compact triples to close binaries and the frequency of disrupted unstable triples.

Both the observed and simulated period distributions of early-type binaries are skewed toward short periods, as shown in Fig. 7. The formation of such OB binaries requires massive disks and significant accretion, which implies very efficient migration. In our baseline model, 33% of the early-B primaries merged with a companion, creating a cliff in the period distribution near $\log P \approx -0.2$. Toward longer periods, the simulated early-B binaries follow a slope $\gamma_P = -0.4$, i.e. a decrease in frequency with $\log P$. The observed samples of close spectroscopic binary companions to O-type stars (Sana et al. 2012; Barbá et al. 2017) and mid-B stars (Abt et al. 1990) yield slopes $\gamma_{\rm P} \approx -0.5$ and 0.0 (Öpik's law), respectively. The observed period distribution of early-B eclipsing binaries provide $\gamma_{\rm P} \approx -0.2$ after correcting for selection effects (Moe & Di Stefano 2013), halfway between the spectroscopic O-type and mid-B samples and matching the simulations.

Analysis of binary statistics from Moe & Di Stefano (2017) in the full range of primary mass M_1 leads to the approximate dependence of the slope on mass as $\gamma_P \approx 0.7 - 0.9 \log M_1$. When we change only the primary mass range in B-type star simulations, the resulting parameter γ_P decreases with increasing mass, e.g. $\gamma_P = -0.15$ for [2-4] $\mathcal{M}_\odot$ and $\gamma_P = -0.50$ for [20-40] $\mathcal{M}_\odot$. However, the period distribution is very sensitive to other parameters such as η, which can be tuned to match the observations.

As shown in Fig. 6, the simulated early-B binaries also exhibit an anti-correlation between P and q, but in a manner that is different from solar-type binaries and consistent with the observed population of massive binaries. For example, there is no deficit of close, extreme mass-ratio companions to early-B primaries in our simulations, unlike the brown dwarf desert observed for solar-type primaries. Moe & Di Stefano (2015a) discovered several eclipsing low-mass pre-MS companions to early-B MS primaries with very short periods $P < 10$ days. They estimated the occurrence rate of very close $q = 0.05$ - 0.15 companions to massive stars is similar to those with $q = 0.15$ - 0.25, consistent with our simulations.

For early-type binaries, the power-law slope γ_q decreases substantially across $\log P = 0$ - 3.2, much more so than for solar-type binaries (Fig. 8). In our baseline early-B model, we compute $\gamma_{q,S} = 0.3$ and $\gamma_{q,L} = -1.3$ for short and long periods, respectively. Although very close companions to OB primaries approximately follow a uniform mass-ratio distribution (Sana et al. 2012; Kobulnicky et al. 2014), there is a large body of evidence that early-type binaries with intermediate separations are substantially skewed toward small mass ratios $q \approx 0.3$ (Rizzuto et al. 2013; Moe & Di Stefano 2015b; Gullikson et al. 2016; Moe & Di Stefano 2017; Murphy et al. 2018). Based on these various surveys, Moe & Di Stefano (2017) estimated $\gamma_{q,L} = -1.5$ for early-B binaries, similar to the results of our baseline model.

The excess twin fraction is substantially reduced for close early-B binaries and quickly diminishes with increasing separation. In our baseline model, we measure $f_{\rm twin,S} = 0.09$ and $f_{\rm twin,L} = 0.06$ across short and long periods, respectively. Based on a compilation of early-type spectroscopic (Sana et al. 2012; Kobulnicky et al. 2014) and eclipsing (Pinsonneault & Stanek 2006; Moe & Di Stefano 2013) binaries, Moe & Di Stefano (2017) estimated $f_{\rm twin,S} \approx 0.08$ - 0.15, depending on primary mass, across $P = 2$ - 20 days. These values are consistent with the simulations and considerably smaller than that measured for close solar-type binaries. Meanwhile, toward longer periods $P \gtrsim 20$ days, Moe & Di Stefano (2017) measured the excess twin fraction of OB binaries to be consistent with zero, placing an upper limit of $f_{\rm twin,L} \lesssim 0.05$, similar to the value in our baseline model.

3.3 Triple systems

Hierarchical systems can be formed in several different ways, e.g. by core fragmentation for the outer subsystem and disk fragmentation for the inner subsystem(s). Our model considers only one process, disk fragmentation, and therefore is not expected to reproduce the full range of real hierarchies. Its relevance is limited to compact hierarchies with outer separations less than ∼50 au where even the outer subsystem can be a product of disk fragmentation and migration. Such triple systems form "from inside out", by adding outer companion to the existing pair and subsequent migration. As stated above, this scenario cannot explain the 2+2 quadruple systems, which must originate in a different way.

Although triple systems are more frequent among massive stars, their statistics and distribution of hierarchical configurations are well established observationally only for solar-type stars, discussed in this Section. Figure 9 illustrates the evolution of a simulated solar-type triple system where the tertiary component has formed early and accreted most of the mass, forming a double twin (both inner and outer mass ratios are close to one). However, this case is atypical because most triple systems form late and their outer companions are less massive compared to both inner stars.

Figure 10 shows the hierarchical distributions of simu-

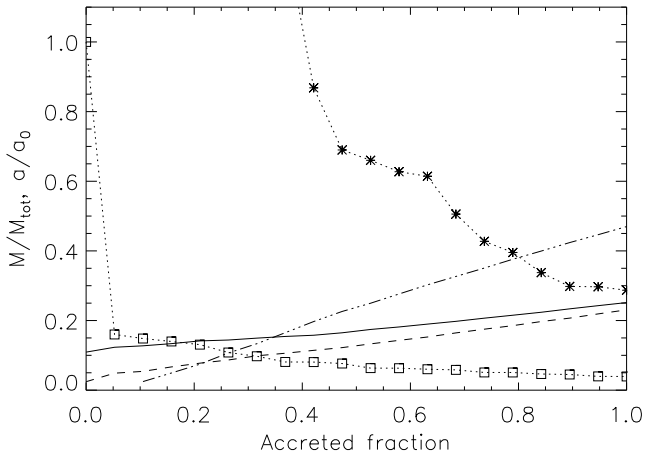

Figure 9. Example of a triple star evolution. As in Figure 1, the masses of the primary and secondary stars in the inner binary, formed in the first accretion episode, are plotted by the full and dashed lines. The tertiary component (dash-dot line) formed at time 0.1 with a semimajor axis of 200 au, much wider than the initial inner binary (outside the plot limit). The final masses of the stars are 0.54, 0.50, and 1.0 $\mathcal{M}_\odot$. The inner and outer separations, relative to the initial inner separation, are plotted by squares and asterisks.

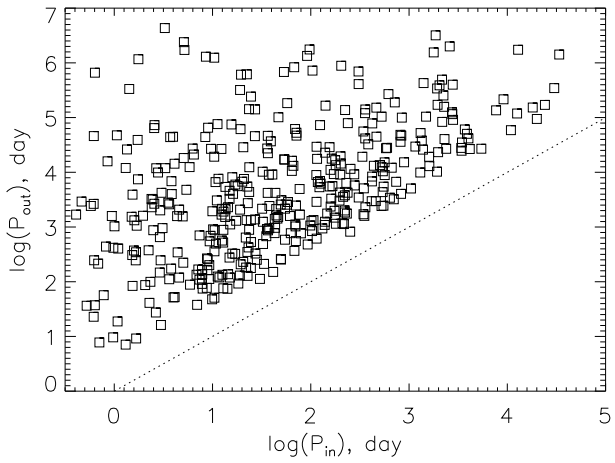

Figure 10. Triple systems with solar-type primaries: periods of inner and outer subsystems (the dotted line marks equality).

lated triple systems with solar-type primaries. The lower envelope of points delineates the adopted crude dynamical stability limit (separation ratio >3). Note the relatively empty lower-left corner, i.e. the paucity of triple systems with very short outer periods $P_{\rm out} < 100$ days. These extremely compact triples must have formed very early, and the difficulty in surviving the migration evolution without becoming dynamical unstable leads to their relative rarity.

Tokovinin et al. (2006) demonstrated that the closest binaries are most likely to be in hierarchical triples. After correcting for incompleteness, they reported $\approx$96% and $\approx$68% of binaries with P = 1-3 days and P = 3-6 days, respectively, have outer tertiaries. The majority of the observed tertiaries to very close binaries are not compact. For

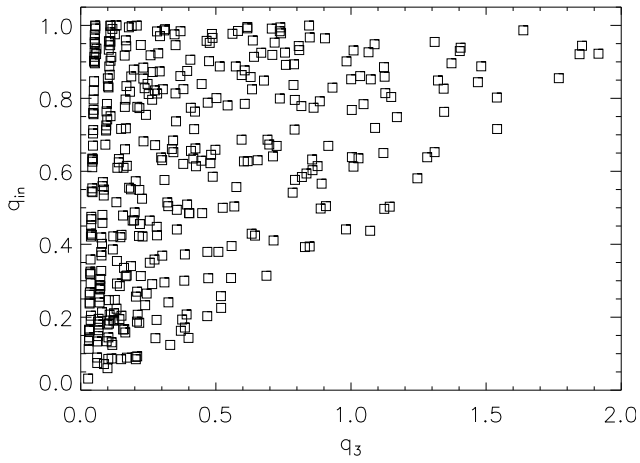

Figure 11. Mass ratios in the outer and inner subsystems of simulated solar-type triple systems.

example, only 5/53 = 9%$\pm$4% of binaries with P = 1-5 days in the 67-pc sample have compact tertiaries within $P_{\rm out} < 10^4$ days, consistent with the value of 13% computed in our baseline model. As discussed in the Introduction, some studies have interpreted the Tokovinin et al. (2006) observations as evidence for hardening the closest binaries via Kozai-Lidov cycles in misaligned triples coupled to tidal friction (Eggleton & Kisseleva-Eggleton 2006; Fabrycky & Tremaine 2007; Naoz & Fabrycky 2014), while others have concluded that the majority of very close binaries derive solely from disk migration (Moe & Kratter 2018). Indeed, our toy model naturally produces very close binaries via disk migration alone. Given the same primary mass, triple star formation requires more mass and accretion, on average, to achieve two fragmentation episodes. The additional mass and accretion facilitates in the inward migration of the inner binary, explaining the anti-correlation between binary period and triple star fraction.

Figure 11 shows the mass ratios of simulated solar-type triples. The outer mass ratio $q_3 = M_3/M_1$ is defined relative to the inner primary component, rather than to the total inner binary mass, as this parameter is easier to determine from observations.[1] The plot can be compared to Figure 5 in Tokovinin (2008). In systems with $q_3 < 1$, the most massive star belongs to the inner binary (hierarchy of Aa,Ab–B type), and in systems with $q_3 > 1$ the tertiary is more massive (hierarchy of A–Ba,Bb type). Only $\approx$12% of simulated triples have $q_3 > 1$. Rare double twins, like the one in Fig. 9, have $q_3 \approx 2$ and are located in the upper right corner of the plot in Figure 11. The median value of q_3 is 0.19, smaller that 0.39 in the real triple stars. The latter, however, is positively biased by observational selection which disfavors discovery of low-mass tertiary companions (see above). Simulated triples with massive tertiaries, like the one in Fig. 9, formed early and migrated more. Consequently, we note an anti-correlation between $P_{\rm out}$ and q_3 for the outer tertiaries, similar to the anti-correlation between

[1] The traditional mass ratio $q_{\rm out} = M_3/(M_1+M_2)$ is related to q_3 as $q_3 = M_3/(M_1+M_2)(1+M_2/M_1) = q_{\rm out}(1+q_{\rm in})$.

P and q for the inner binaries. Overall, the tertiaries are weighted toward small mass ratios $q_3 < 0.3$ and do not exhibit an excess of twins. According to our model, if a twin binary within $a < 10$ au is observed, than it is unlikely that either of the components will have their own subcompanions.

The lower-right corner of the plot is empty, meaning that there are no simulated triples where both secondary and tertiary components have small masses. In our model, triple stars which formed inside-out by cascade of disk fragmentations with subsequent migration must have $q_{\rm in} \gtrsim 0.5q_3$ or, equivalently, $M_3 \lesssim 2M_2$. However, in the Borkovits et al. (2016) sample of compact triples, where the ratio of eclipse depths indicates the mass ratio $q_{\rm in}$ of the inner eclipsing binary while eclipse timing variations provide the masses M_1+M_2 and M_3, there are a handful of A–Ba,Bb triples with $q_3 > 2$. For example, KOI-126 (KIC 5897826) contains a triple eclipsing nearly coplanar A–Ba,Bb triple with $q_3 = 5.6$ in which a very close pair of low-mass M-dwarfs with $M_{\rm Ba} = 0.24\,\mathcal{M}_\odot$, $M_{\rm Bb} = 0.21\,\mathcal{M}_\odot$, and $P_{\rm in} = 1.78$ days orbits a G1 IV primary with $M_{\rm A} = 1.35\ \mathcal{M}_\odot$ at $P_{\rm out} = 33.9$ days (Carter et al. 2011). The inner binary likely formed at very early times, and therefore migrated toward $P_{\rm in} \approx 2$ days while evolving into a near twin with $q_{\rm in} \approx 0.8$, and then the outer tertiary fragmented, accreted most of the remaining mass to $M_{\rm A} = 1.35\,\mathcal{M}_\odot$, and migrated to $P_{\rm out} \approx 34$ days. Our model cannot produce such A–Ba,Bb triples with $q_3 > 2$ because we assume most of the mass is accreted by the inner binary if its combined mass is less than that of the tertiary. In any case, only a small minority of compact triples in the Borkovits et al. (2016) sample have $q_3 > 2$, most of which have $P_{\rm in} < 5$ days and $M_{\rm A} > 1.3\mathcal{M}_\odot$ (not true solar-type primaries per our definition). The majority of their solar-type triples have large $q_{\rm in}$ and small q_3, consistent with the parameter space of our models as shown in Fig. 11.

3.4 Variation of the parameters

We have chosen the default parameters of the toy model (Table 1) to mimic the real binary statistics, at least qualitatively (one cannot expect a perfect match from our crude model). Here we explore how changes of the parameters affect the outcome of the simulations. Supplementary models with these changes were introduced above in Section 2. The statistical parameters are described in Table 2. Table 3 shows the statistics of simulated solar-type binaries resulting from supplementary models. The default simulations were performed for 20,000 binaries. Then we change one parameter at a time, generate 4,000 binaries, and determine their statistics. The last column shows the modified parameter values and, in brackets, its default value. Table 4 gives similar information for B-type stars. For reference, the observed parameters are given in the first line of both tables.

The toy model is relatively robust to variation of many parameters. For example, model predictions for the companion frequency and twin fraction are relatively insensitive to many parameters except $f_{\rm bin}$. However, we found that the parameters that determine the migration rate are critical and affect the results strongly. Those are the migration coefficient η, the companion seed mass f_{m20}, and its growth parameter $f_{\rm m2max}$. Both small seed companion mass and limited growth strongly increase the migration (and, for B-type stars, the merger rate). As a result, small mass ratios become dominant (negative γ_q). The same effect is produced by increasing the migration rate η. The default combination of these parameters was chosen by trial and error to get realistic outcome of the simulation. Other combinations are not precluded, but the strong influence of these three parameters and their inter-relation is evident. The reason is that migration is fastest just after the companion's formation, and its initial mass matters. When the migration rate increases (larger η, smaller f_{m20}, and/or smaller $f_{\rm m2max}$), the merger rate also increases and thus the close binary fraction drops, which is especially evident for B-type stars.

The following parameters are less critical. The initial seed mass of the primary f_{m0} affects mostly the twin fraction (more twins for smaller seeds). For solar-type binaries, the number of accretion episodes $K_{\rm step}$ affects the twin fraction (more twins if less episodes), $\gamma_{q,L}$ at long periods (decreases with increasing $K_{\rm step}$), and the slope of the period distribution (decrease γ_P), which means stronger overall migration with more episodes. The effect of changing the companion frequency $f_{\rm bin}$ is obvious: more binaries and triples, more disruptions, but almost no influence on the distributions of the mass ratio and period for solar-type stars (for B-type stars, there is a minor effect).

Increasing the fragmentation probability in the first episodes ($\gamma_{\rm frag} = -0.5$) increases the average mass ratio and the twin fraction because companions have more time to grow. Obviously, $\gamma_{\rm frag} = 0.5$ has the inverse effect and yields less massive companions. The prevalence of close solar-type twins strongly suggests accretion rates are large, or at least highly variable, at early times, whereas models in which the mass accretion rate, and therefore probability of disk fragmentation, steadily increase in time are disfavored. Other parameters such as period distribution and multiplicity fraction remain almost unaffected by $\gamma_{\rm frag}$. The parameter β also affects mostly the mass ratio distribution (more twins for $\beta = 0.5$, opposite for $\beta = 0.9$).

Finally, replacing disruptions by unfolding and shrinkage of the inner binary in `Fold1` has almost no effect, except the increased fraction of triples. For solar-type binaries, the fraction of disruptions (or unfoldings) is only 0.03.

4 SUMMARY AND DISCUSSION

Our toy model encompasses the stochastic nature of disk fragmentation (which provide the initial conditions; Section 2.1), subsequent accretion onto the binary components (mass growth; Section 2.2), and angular momentum exchanges and losses (migration; Section 2.3). We do not yet have detailed physical models for these various processes that fully and self-consistently incorporate all of the underlying physics, e.g., eccentric orbits, misaligned disks, magnetic fields, variable and chaotic accretion, and outflows and jets. Motivated by observational constraints and hydrodynamic simulations of certain ideal scenarios, our toy model instead utilizes a few simple analytic prescriptions with inherent variability to encapsulate the complexity and stochasticity of disk fragmentation, accretion, and migration.

Our toy model naturally reproduces 14 observed features of close multiples: (1) a small ratio TF/BF $\approx 5\%$ of compact triples to close binaries for solar-type systems, (2)

Table 3. Supplementary models for solar-type stars

Model	CF	BF	TF	$f_{\rm disrupt}$	$f_{\rm merge}$	$\gamma_{q,S}$	$f_{\rm twin,S}$	$\gamma_{q,L}$	$f_{\rm twin,L}$	γ_P	Comment
Observed	...	*0.24*	*0.02*	...	...	*0.8*	*0.24*	*0.3*	*0.16*	*0.7*	
Baseline	**0.37**	**0.30**	**0.03**	**0.03**	**0.00**	**1.5**	**0.20**	**0.2**	**0.15**	**0.71**	Default
PrimSeed1	0.39	0.32	0.03	0.03	0.01	1.5	0.29	0.2	0.25	0.55	$f_{\rm m0} = 0.05$ (0.1)
PrimSeed2	0.38	0.30	0.03	0.03	0.00	1.4	0.06	0.2	0.04	0.74	$f_{\rm m0} = 0.15$ (0.1)
CompSeed1	0.37	0.22	0.02	0.03	0.00	6.0	0.63	1.4	0.21	4.11	$f_{\rm m20} = 0.5$ (0.25)
CompSeed2	0.16	0.14	0.01	0.02	0.16	0.5	0.08	−0.5	0.12	−0.18	$f_{\rm m20} = 0.1$ (0.25)
MaxAcc1	0.39	0.27	0.02	0.03	0.00	2.4	0.33	1.2	0.18	2.13	$f_{\rm m2max} = 2.0$ (1.0)
MaxAcc2	0.28	0.24	0.02	0.03	0.08	0.4	0.11	0.0	0.06	−0.09	$f_{\rm m2max} = 0.5$ (1.0)
Eta1	0.38	0.21	0.02	0.02	0.00	1.7	0.14	0.9	0.15	1.33	$\eta = [-1, 3]$ ([0,3])
Eta2	0.35	0.31	0.03	0.04	0.02	1.2	0.14	−1.4	0.10	0.00	$\eta = [1, 3]$ ([0,3])
Step1	0.39	0.28	0.02	0.03	0.00	1.9	0.24	0.5	0.20	1.22	$K_{\rm step} = 10$ (20)
Step2	0.37	0.31	0.02	0.04	0.02	1.3	0.13	0.0	0.08	0.30	$K_{\rm step} = 40$ (20)
Mult1	0.27	0.22	0.01	0.02	0.00	1.4	0.18	0.4	0.12	0.74	$f_{\rm bin} = 0.2$ (0.3)
Mult2	0.57	0.43	0.06	0.08	0.01	1.3	0.18	0.4	0.15	0.81	$f_{\rm bin} = 0.5$ (0.3)
Frag1	0.40	0.34	0.02	0.04	0.00	2.4	0.28	0.9	0.25	0.63	$\gamma_{\rm frag} = -0.5$ (0)
Frag2	0.38	0.28	0.03	0.03	0.00	1.1	0.09	−0.5	0.08	0.67	$\gamma_{\rm frag} = 0.5$ (0)
Beta1	0.39	0.31	0.03	0.04	0.00	1.5	0.31	0.2	0.22	0.69	$\beta = 0.5$ (0.7)
Beta2	0.39	0.30	0.03	0.03	0.00	1.2	0.06	0.5	0.04	0.74	$\beta = 0.9$ (0.7)
Fold1	0.43	0.28	0.06	0.04	0.00	1.3	0.10	0.5	0.04	0.74	Unfold and shrink

Table 4. Supplementary models for B-type stars

Model	CF	BF	TF	$f_{\rm disrupt}$	$f_{\rm merge}$	$\gamma_{q,S}$	$f_{\rm twin,S}$	$\gamma_{q,L}$	$f_{\rm twin,L}$	γ_P	Comment
Observed	...	*0.50*	*0.10*	...	...	*−0.2*	*0.12*	*−1.5*	*<0.05*	*−0.2*	
Baseline	**0.75**	**0.56**	**0.13**	**0.45**	**0.33**	**0.3**	**0.09**	**−1.3**	**0.06**	**−0.40**	Default
PrimSeed1	0.71	0.53	0.12	0.46	0.36	0.5	0.19	−1.2	0.09	−0.35	$f_{\rm m0} = 0.05$ (0.1)
PrimSeed2	0.77	0.56	0.14	0.44	0.32	0.4	−0.02	−1.5	0.02	−0.22	$f_{\rm m0} = 0.15$ (0.1)
CompSeed1	1.23	0.73	0.33	0.51	0.08	1.4	0.12	−0.6	0.10	0.14	$f_{\rm m20} = 0.5$ (0.25)
CompSeed2	0.13	0.11	0.00	0.15	0.76	−0.7	0.06	−1.3	0.07	−0.74	$f_{\rm m20} = 0.1$ (0.25)
MaxAcc1	1.07	0.69	0.25	0.50	0.16	0.9	0.10	−1.0	0.07	−0.17	$f_{\rm m2max} = 2.0$ (1.0)
MaxAcc2	0.26	0.21	0.02	0.26	0.66	−0.8	0.06	−2.1	0.01	−0.58	$f_{\rm m2max} = 0.5$ (1.0)
Eta1	1.31	0.53	0.32	0.42	0.03	1.2	0.08	0.9	0.10	0.56	$\eta = [-1, 3]$ ([0, 4])
Eta2	0.18	0.16	0.01	0.23	0.72	−3.5	0.00	0.0	0.00	−0.43	$\eta = [1, 5]$ ([0, 4])
Step1	1.01	0.66	0.22	0.50	0.19	0.7	0.12	−0.5	0.10	−0.16	$K_{\rm step} = 25$ (50)
Step2	0.46	0.38	0.05	0.36	0.50	−0.3	0.08	−2.5	0.00	−0.74	$K_{\rm step} = 100$ (50)
Mult1	0.37	0.32	0.03	0.12	0.29	0.3	0.08	−1.7	0.07	−0.50	$f_{\rm bin} = 0.8$ (2.0)
Mult2	0.88	0.61	0.18	0.57	0.31	0.4	0.10	−1.0	0.06	−0.42	$f_{\rm bin} = 2.5$ (2.0)
Frag1	0.67	0.53	0.11	0.47	0.39	1.3	0.19	−1.0	0.16	−0.53	$\gamma_{\rm frag} = -0.5$ (0)
Frag2	0.82	0.57	0.16	0.43	0.29	−0.3	0.06	−1.3	0.01	−0.36	$\gamma_{\rm frag} = 0.5$ (0)
Beta1	0.74	0.55	0.13	0.45	0.34	0.2	0.18	−1.6	0.15	−0.40	$\beta = 0.5$ (0.7)
Beta2	0.75	0.56	0.14	0.46	0.33	0.6	−0.01	−1.0	0.01	−0.47	$\beta = 0.9$ (0.7)
Fold1	1.46	0.42	0.40	0.49	0.29	−0.4	0.01	−1.3	−0.02	−0.11	Unfold and shrink

which increases to TF/BF $\approx 20\%$ for early-B primaries; (3) an increasing solar-type binary period distribution ($\gamma_{\rm P} = {\rm d}N/{\rm dlog}P = 0.7$), (4) whereas early-B binaries are skewed toward very short periods ($\gamma_{\rm P} = \approx -0.2$); (5) the brown dwarf desert, i.e., the paucity of low-mass companions to solar-type primaries at short periods $P \lesssim 100$ days, (6) but a prevalence of brown dwarf companions at longer periods; (7) the existence of $q = 0.05$-0.10 companions to early-B primaries with very short periods $P < 10$ days; (8) a large excess fraction $f_{\rm twin,S} \approx 0.24$ of twins ($q > 0.95$) among short-period solar-type binaries, (9) which decreases linearly in frequency with $\log P$; (10) a reduced but non-zero excess twin fraction $f_{\rm twin,S} \approx 0.12$ among the closest early-B binaries, but (11) no excess twins to early-B primaries beyond $P \gtrsim 50$ days ($f_{\rm twin,L} < 0.05$); (12) a relatively uniform or slightly increasing mass-ratio distribution across $q = 0.3$-0.95 both for solar-type binaries ($\gamma_{\rm q} \approx 0.5$) and (13) for short-period companions to early-B stars ($\gamma_{\rm q,S} \approx 0.0$), but (14) wider companions to early-B stars that are weighted toward small mass ratios ($\gamma_{\rm q,L} \approx -1.5$).

Twins correspond to binaries that formed early and experienced a runaway growth of the mass ratio. This process is almost scale-free, i.e. independent of the total mass. However, a significant fraction of massive binaries that formed early have merged, reducing the fraction of twins among massive stars. The fraction of twins slowly decreases with increasing period. Early findings that solar-type twins have only short periods $P < 30$ d (Lucy & Ricco 1979; Tokovinin

2000) is likely a selection effect because double-lined twin spectroscopic binaries require a high spectroscopic resolution to split the lines. However, it is now established that the excess twin population exists among visual binaries (Moe & Di Stefano 2017; El-Badry et al. 2019), in line with our predictions.

The brown dwarf desert is a natural consequence of accretion-driven migration. A substellar companion inevitably grows into the stellar-mass regime while migrating inward. Only companions formed by disk fragmentation at the very end of the mass assembly have a chance to remain substellar (Kratter et al. 2010), but they migrate little.

Our model predicts a large number of mergers during formation of massive stars owing to strong accretion and, consequently, fast migration. The latter also translates into the period distribution that grows toward short periods and falls abruptly at the minimum period corresponding to merger. Early mergers help to build up stellar masses more gradually, compared to a simple accretion. Very massive stars have a short lifetime, and assembling their mass rapidly by accretion implies very high (probably unrealistic) accretion rates. Formation of massive stars by merging has been suggested several times as a way to alleviate this problem (e.g. Bonnell et al. 1998). However, direct collisions between stars require a very high stellar density if they happen in a cluster, or the existence of many compact and dynamically unstable triple systems. In our scenario, formation of companions, their migration, and merging is driven only by accretion. Massive stars are assembled from gas, but part of this gas is delivered in the form of companions. The lifetime of companions is longer than the lifetime of massive merger products, hence mergers relax the requirement on the accretion rate need to form massive stars.

It is most remarkable that the toy models for solar-type and B-type stars have similar critical parameters that define the migration rate and the mass-ratio distribution (η, f_{m20}, f_{m2max}, and β). The differences in the close-binary statistics of those populations can be explained only by the difference in their mass, using the same prescriptions with similar parameters.

Accretion-driven migration is inevitably associated with the growth of the mass ratio. Existence of close binaries with small q has always been a challenge to this theory. The toy model addresses this challenge by postulating that companions form during the whole period of mass assembly, not at the same time as the primary star. In young pre-MS eclipsing binaries, the components are not exactly coeval (Stassun et al. 2008; Gómez Maqueo Chew et al. 2012). Moreover, the migration is strongest at the beginning, in the low-q regime. Our crude prescription allows low-mass companions to migrate to short periods before substantial mass growth. The physics of companion growth and migration in the low-q regime is complex and unlikely to be captured correctly by our prescription. However, the prediction that low-mass companions can rapidly migrate to short separations is one of the results of our study.

It is instructive to compare our results with those of Bate (2000). He studied the evolution of seed binaries immersed in co-rotating cores and accreting most of their mass in a deterministic and conservative way according to the prescriptions of Bate & Bonnell (1997). In common with this study, Bate predicted asymptotic growth of the mass ratio towards $q = 1$ (formation of twins) and the brown dwarf desert at short periods. However, his model is unable to produce close massive binaries with small q, while the initial orbital separations tend to increase, rather than shrink, owing to the conservation of angular momentum. In contrast, our toy model postulates orbit shrinking (negative and random η), assumes companion formation at random times, rather than simultaneously with the primary, and includes mergers. This helps us to reach a qualitative agreement of the P, q statistics with observations. However, our model hides the complexity of the real binary evolution behind crude prescriptions with random parameters, while Bate based his study on the actual, albeit incomplete, treatment of the binary evolution. We hope that in the future both approaches will converge and that our study will motivate further simulations of accreting binaries leading to better prescriptions for their evolution.

M.M. acknowledges financial support from NASA under Grant No. ATP-170070.

REFERENCES

Abt H. A., Gomez A. E., Levy S. G., 1990, ApJS, 74, 551
Ansdell M., et al., 2016, ApJ, 828, 46
Ansdell M., et al., 2018, ApJ, 859, 21
Artymowicz P., 1983, Acta Astronomica, 33, 223
Artymowicz P., Lubow S. H., 1996, ApJ, 467, L77
Artymowicz P., Clarke C. J., Lubow S. H., Pringle J. E., 1991, ApJ, 370, L35
Badenes C., et al., 2018, ApJ, 854, 147
Bally J., 2016, ARA&A, 54, 491
Barbá R. H., Gamen R., Arias J. I., Morrell N. I., 2017, in Eldridge J. J., Bray J. C., McClelland L. A. S., Xiao L., eds, IAU Symposium Vol. 329, The Lives and Death-Throes of Massive Stars. pp 89–96, doi:10.1017/S1743921317003258
Bate M. R., 1998, ApJ, 508, L95
Bate M. R., 2000, MNRAS, 314, 33
Bate M. R., 2011, MNRAS, 417, 2036
Bate M. R., 2014, MNRAS, 442, 285
Bate M. R., 2019, MNRAS, 484, 2341
Bate M. R., Bonnell I. A., 1997, MNRAS, 285, 33
Bate M. R., Bonnell I. A., Price N. M., 1995, MNRAS, 277, 362
Bate M. R., Bonnell I. A., Bromm V., 2002, MNRAS, 336, 705
Behrend R., Maeder A., 2001, A&A, 373, 190
Boley A. C., Hayfield T., Mayer L., Durisen R. H., 2010, Icarus, 207, 509
Bonnell I. A., Bate M. R., 2005, MNRAS, 362, 915
Bonnell I. A., Bate M. R., Zinnecker H., 1998, MNRAS, 298, 93
Borkovits T., Hajdu T., Sztakovics J., Rappaport S., Levine A., Bíró I. B., Klagyivik P., 2016, MNRAS, 455, 4136
Boss A. P., 1986, ApJS, 62, 519
Boss A. P., 1998, Annual Review of Earth and Planetary Sciences, 26, 53
Brandt T. D., 2018, ApJS, 239, 31
Carter J. A., et al., 2011, Science, 331, 562
Cesaroni R., Galli D., Lodato G., Walmsley C. M., Zhang Q., 2007, in Reipurth B., Jewitt D., Keil K., eds, Protostars and Planets V. p. 197 (arXiv:astro-ph/0603093)
Clarke C. J., 2009, MNRAS, 396, 1066
Csizmadia S., et al., 2015, A&A, 584, A13
Czekala I., Chiang E., Andrews S. M., Jensen E. L. N., Torres G., Wilner D. J., Stassun K. G., Macintosh B., 2019, arXiv e-prints, p. arXiv:1906.03269
Doğan S., Nixon C., King A., Price D. J., 2015, MNRAS, 449, 1251

Dunham M. M., Vorobyov E. I., Arce H. G., 2014, MNRAS, 444, 887
Dunhill A. C., Cuadra J., Dougados C., 2015, MNRAS, 448, 3545
Duquennoy A., Mayor M., 1991, A&A, 500, 337
Eggleton P. P., 1983, ApJ, 268, 368
Eggleton P. P., Kisseleva-Eggleton L., 2006, Ap&SS, 304, 75
El-Badry K., Rix H.-W., 2019, MNRAS, 482, L139
El-Badry K., Rix H.-W., Tian H., Duchêne G., Moe M., 2019, arXiv e-prints, p. arXiv:1906.10128
Fabrycky D., Tremaine S., 2007, ApJ, 669, 1298
Farris B. D., Duffell P., MacFadyen A. I., Haiman Z., 2014, ApJ, 783, 134
Frank A., et al., 2014, in Beuther H., Klessen R. S., Dullemond C. P., Henning T., eds, Protostars and Planets VI. p. 451 (arXiv:1402.3553), doi:10.2458/azu_uapress_9780816531240-ch020
Froebrich D., Schmeja S., Smith M. D., Klessen R. S., 2006, MNRAS, 368, 435
Girichidis P., Federrath C., Allison R., Banerjee R., Klessen R. S., 2012, MNRAS, 420, 3264
Goicovic F. G., Sesana A., Cuadra J., Stasyszyn F., 2017, MNRAS, 472, 514
Gómez Maqueo Chew Y., Stassun K. G., Prša A., Stempels E., Hebb L., Barnes R., Heller R., Mathieu R. D., 2012, ApJ, 745, 58
Goodman J., Tan J. C., 2004, ApJ, 608, 108
Goodwin S. P., Whitworth A. P., Ward-Thompson D., 2004, A&A, 414, 633
Grether D., Lineweaver C. H., 2006, ApJ, 640, 1051
Gullikson K., Kraus A., Dodson-Robinson S., 2016, AJ, 152, 40
Haemmerlé L., Eggenberger P., Meynet G., Maeder A., Charbonnel C., 2016, A&A, 585, A65
Haemmerlé L., et al., 2019, A&A, 624, A137
Hanawa T., Ochi Y., Ando K., 2010, ApJ, 708, 485
Hartigan P., Edwards S., Ghandour L., 1995, ApJ, 452, 736
Hartmann L., Kenyon S. J., 1996, ARA&A, 34, 207
Hartmann L., Herczeg G., Calvet N., 2016, ARA&A, 54, 135
Hayasaki K., Saito H., Mineshige S., 2013, Publications of the Astronomical Society of Japan, 65, 86
Hurley J. R., Aarseth S. J., Shara M. M., 2007, ApJ, 665, 707
Ivanov P. B., Papaloizou J. C. B., Paardekooper S. J., Polnarev A. G., 2015, A&A, 576, A29
Kamp I., Dullemond C. P., 2004, ApJ, 615, 991
Kamp I., van Zadelhoff G. J., 2001, A&A, 373, 641
Kippenhahn R., Meyer-Hofmeister E., 1977, A&A, 54, 539
Kobulnicky H. A., et al., 2014, ApJS, 213, 34
Kounkel M., et al., 2019, AJ, 157, 196
Kratter K., Lodato G., 2016, ARA&A, 54, 271
Kratter K. M., Matzner C. D., 2006, MNRAS, 373, 1563
Kratter K. M., Matzner C. D., Krumholz M. R., 2008, ApJ, 681, 375
Kratter K. M., Matzner C. D., Krumholz M. R., Klein R. I., 2010, ApJ, 708, 1585
Kraus A. L., Ireland M. J., Martinache F., Lloyd J. P., 2008, ApJ, 679, 762
Kraus A. L., Ireland M. J., Martinache F., Hillenbrand L. A., 2011, ApJ, 731, 8
Kroupa P., 1995, MNRAS, 277, 1491
Krumholz M. R., Klein R. I., McKee C. F., Offner S. S. R., Cunningham A. J., 2009, Science, 323, 754
Lucy L. B., Ricco E., 1979, AJ, 84, 401
Machida M. N., Omukai K., Matsumoto T., Inutsuka S.-I., 2009, MNRAS, 399, 1255
Mathieu R. D., 1994, ARA&A, 32, 465
McKee C. F., Tan J. C., 2003, ApJ, 585, 850
Melo C. H. F., 2003, A&A, 410, 269
Moe M., Di Stefano R., 2013, ApJ, 778, 95
Moe M., Di Stefano R., 2015a, ApJ, 801, 113
Moe M., Di Stefano R., 2015b, ApJ, 810, 61
Moe M., Di Stefano R., 2017, ApJS, 230, 15
Moe M., Kratter K. M., 2018, ApJ, 854, 44
Moe M., Kratter K. M., Badenes C., 2019, ApJ, 875, 61
Muñoz D. J., Miranda R., Lai D., 2019, ApJ, 871, 84
Murphy S. J., Moe M., Kurtz D. W., Bedding T. R., Shibahashi H., Boffin H. M. J., 2018, MNRAS, 474, 4322
Murray S. D., Clarke C. J., Pringle J. E., 1991, ApJ, 383, 192
Naoz S., Fabrycky D. C., 2014, ApJ, 793, 137
Natta A., Testi L., Alcalá J. M., Rigliaco E., Covino E., Stelzer B., D'Elia V., 2014, A&A, 569, A5
Nixon C., King A., Price D., 2013, MNRAS, 434, 1946
Offner S. S. R., Kratter K. M., Matzner C. D., Krumholz M. R., Klein R. I., 2010, ApJ, 725, 1485
Peters T., Klessen R. S., Mac Low M.-M., Banerjee R., 2010, ApJ, 725, 134
Pinsonneault M. H., Stanek K. Z., 2006, ApJ, 639, L67
Pols O. R., Marinus M., 1994, A&A, 288, 475
Press W. H., Teukolsky S. A., 1977, ApJ, 213, 183
Raghavan D., et al., 2010, ApJS, 190, 1
Reipurth B., Bally J., 2001, ARA&A, 39, 403
Reipurth B., Clarke C., 2001, AJ, 122, 432
Rigliaco E., Pascucci I., Gorti U., Edwards S., Hollenbach D., 2013, ApJ, 772, 60
Rizzuto A. C., et al., 2013, MNRAS, 436, 1694
Roedig C., Sesana A., 2014, MNRAS, 439, 3476
Sana H., et al., 2012, Science, 337, 444
Shahaf S., Mazeh T., 2019, MNRAS, 487, 3356
Sheehan P. D., Eisner J. A., 2014, ApJ, 791, 19
Sheehan P. D., Eisner J. A., 2017, ApJ, 851, 45
Sollima A., 2008, MNRAS, 388, 307
Stassun K. G., Mathieu R. D., Cargile P. A., Aarnio A. N., Stempels E., Geller A., 2008, Nature, 453, 1079
Tanaka K. E. I., Omukai K., 2014, MNRAS, 439, 1884
Tang Y., MacFadyen A., Haiman Z., 2017, MNRAS, 469, 4258
Tobin J. J., et al., 2016, Nature, 538, 483
Tohline J. E., 2002, ARA&A, 40, 349
Tokovinin A. A., 2000, A&A, 360, 997
Tokovinin A., 2008, MNRAS, 389, 925
Tokovinin A., 2014, AJ, 147, 86
Tokovinin A., 2017, ApJ, 844, 103
Tokovinin A., Thomas S., Sterzik M., Udry S., 2006, A&A, 450, 681
Umbreit S., Burkert A., Henning T., Mikkola S., Spurzem R., 2005, ApJ, 623, 940
Wagner K., Apai D., Kratter K. M., 2019, ApJ, 877, 46
White R. J., Ghez A. M., 2001, ApJ, 556, 265
Williams J. P., Cieza L. A., 2011, ARA&A, 49, 67
Young M. D., Clarke C. J., 2015, MNRAS, 452, 3085
Zhao B., Li Z.-Y., 2013, ApJ, 763, 7
de Val-Borro M., Gahm G. F., Stempels H. C., Pepliński A., 2011, MNRAS, 413, 2679

5 SUPPLEMENTARY MATERIAL

The IDL code used to simulate binaries is provided in `toy-model.tar.gz`.

This paper has been typeset from a TEX/LATEX file prepared by the author.